propagation, with the indication that it cannot be ignored. For the case of coupled waveguides, it was noted that the coupling is practically unaffected when the optical axes of one of the waveguides are rotated with respect to the coordinate-system axes.

## REFERENCES


[1] N. Schulz, K. Bierwirth, and F. Arndt, "Finite-difference analysis of integrated optical waveguides without spurious mode solutions," *Electron. Lett.*, vol. 22, no. 18, pp. 963–965, Aug. 1986.

[2] C. L. da S. S. Sobrinho and A. J. Giarola, "Analysis of an infinite array of rectangular anisotropic dielectric waveguides using the finite-difference method," *IEEE Trans. Microwave Theory Tech.*, vol. 40, pp. 1021–1025, May 1992.

[3] S. Xiao and R. Vahldieck, "An efficient 2-D FDTD algorithm using real values," *IEEE Microwave Guided Wave Lett.*, vol. 3, pp. 127–129, May 1993.

[4] K. Hayata, M. Koshiba, M. Eguchi, and M. Suzuki, "Vectorial finite-element method without any spurious solutions for dielectric waveguiding problems using transverse magnetic-field component," *IEEE Trans. Microwave Theory Tech.*, vol. MTT-34, pp. 1120–1124, Nov. 1986.

[5] J. Huang and K. Wu, "Toward a generalized TLM algorithm for solving arbitrary reciprocal and nonreciprocal planar structures," *IEEE Trans. Microwave Theory Tech.*, vol. 44, pp. 1508–1511, Aug. 1996.


# Scattering by an Infinite Elliptic Dielectric Cylinder Coating Eccentrically a Circular Metallic or Dielectric Cylinder

Stylianos P. Savaidis and John A. Roumeliotis

***Abstract*—In this paper, the scattering of a plane electromagnetic wave by an infinite elliptic dielectric cylinder, coating eccentrically a circular metallic or dielectric inner cylinder, is treated. The electromagnetic field is expressed in terms of both circular and elliptical–cylindrical wave functions, which are connected with one another by well-known expansion formulas. Translational addition theorems for circular cylindrical wave functions are also used. If the solution is specialized to small values of $h = k_2 c/2$, where $k_2$ is the wavenumber of the elliptic dielectric cylinder and $c$ its interfocal distance, semianalytical expressions of the form $S(h) = S(0)[1 + gh^2 + O(h^4)]$ are obtained for the scattered field and the various scattering cross sections of this configuration. The coefficients $g$ are independent of $h$. Both polarizations are considered for normal incidence. Graphical results for the scattering cross sections are given for various values of the parameters.**

***Index Terms*—Eccentric elliptical–circular cylinders, scattering.**

## I. INTRODUCTION

Scattering from composite bodies is often used for detecting their internal structure. Analytical solution of such problems is severely limited by the shape of boundaries. For complicated geometries, various numerical methods can be used.

Scattering from a dielectric elliptic cylinder coated with another nonconfocal dielectric one, or from two parallel dielectric elliptic cylinders, is examined in [1] and [2], respectively.

In this paper, the scattering of an electromagnetic plane wave by an infinite elliptic dielectric cylinder containing an off-axis metallic or dielectric circular inner cylinder, is considered. The geometry of the scatterer, shown in Fig. 1, is a perturbation of the eccentric circular one, with radii $R_1$ and $R_2$. All materials are lossless. Both polarizations are considered for normal incidence.

Using translational addition theorems for circular cylindrical wave functions [3] and expansion formulas between circular and elliptical (Mathieu) wave functions [3], [4], we conclude (after the satisfaction of the boundary conditions and some manipulation) with two infinite sets of linear nonhomogeneous equations for the expansion coefficients of the electromagnetic field inside the elliptic dielectric cylinder.

For general values of $h = k_2 c/2$ these sets can be only solved numerically by truncation, but for $h \ll 1$, a semianalytical solution is possible. After very lengthy and laborious, but straightforward calculations, we obtain expressions of the form $S(h) = S(0)[1 + gh^2 + O(h^4)]$ for the scattered field and the scattering cross sections. The coefficients $g$ are independent of $h$, while $S(0)$ corresponds to the eccentric circular problem. The main advantage is that these expressions are valid for each small $h$, *free* of Mathieu functions, while all purely numerical techniques require repetition of the calculation for each different $h$, a very complicated task due to these functions.

This advantage distinguishes this paper from [1], [5], which contribute more general geometries. By using the solutions of [1] and [5] to obtain our numerical results, one should repeat the very complicated steps containing the calculation of the various Mathieu functions for each different $h$.

Apart from its mathematical interest, the elliptical–circular combination of this problem may enhance or decrease the various scattering cross sections, as compared to those for the eccentric circular geometry.

The solution of this problem is much more complex and lengthy than that in the corresponding coaxial one [6] due to the eccentricity, the presence of a dielectric inner cylinder in one case here, and the use of different permeabilities for the various regions in this paper. In [6], the wavenumbers in the elliptic dielectric cylinder and the surrounding medium were also nearly equal ($h \cong h_2$ there), while here they are different.

## II. METALLIC INNER CYLINDER

### A. $E$-Wave Polarization

*1) Calculation of the Field:* We begin with a metallic inner cylinder and the $E$-wave polarization. The incident plane wave normally impinging on the $z$-axis has the form [3], [4]

$$E_z^{inc} = \sqrt{8\pi} \sum_{m=0}^{\infty} j^{-m} \left[ \frac{Se_m(h_3, \cos\psi)}{M_m^e(h_3)} \times Se_m(h_3, \cos\theta) Je_m(h_3, \cosh\mu) + \frac{So_m(h_3, \cos\psi)}{M_m^o(h_3)} So_m(h_3, \cos\theta) \times Jo_m(h_3, \cosh\mu) \right], \qquad h_3 = \frac{k_3 c}{2} \quad (1)$$

with $\mu$, $\theta$ the transverse elliptical–cylindrical coordinates with respect to $xOy$, $Je_m(Jo_m)$ the even (odd) radial Mathieu functions of the first kind, and $Se_m(So_m)$ the even (odd) angular Mathieu functions. The normalization constants $M_m^{e(o)}$ are given in [4]. The angle $\psi$ defines the direction of incidence with respect to $x$. The time dependence $\exp(j\omega t)$ is suppressed throughout.

Manuscript received January 23, 1996; revised June 20, 1997.

The authors are with the Department of Electrical and Computer Engineering, National Technical University of Athens, Athens 15773, Greece.

Publisher Item Identifier S 0018-9480(97)07114-7.

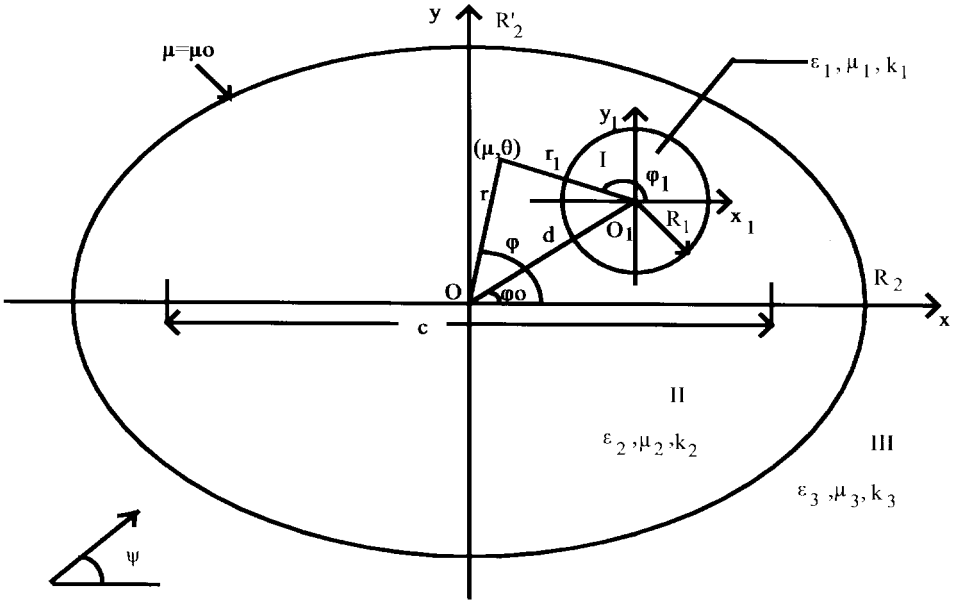


Fig. 1. Geometry of the scatterer.

The scattered field is expressed as

$$E_z^{sc} = \sum_{m=0}^{\infty} [P_m Se_m(h_3, \cos\theta) He_m(h_3, \cosh\mu) + Q_m So_m(h_3, \cos\theta) Ho_m(h_3, \cosh\mu)] \quad (2)$$

where $He_m(Ho_m)$ are the even (odd) radial Mathieu functions of the fourth kind [the superscript (2) is omitted for simplicity].

The field in Region II, expressed in terms of circular cylindrical wave functions with respect to $x_1O_1y_1$, and satisfying the boundary condition $E_z^{\mathrm{II}} = 0$ at $r_1 = R_1$, is

$$E_z^{\mathrm{II}} = \sum_{i=0}^{\infty} [J_i(k_2 r_1) N_i(x_3) - J_i(x_3) N_i(k_2 r_1)] \times (A_i \cos i\varphi_1 + B_i \sin i\varphi_1), \qquad x_3 = k_2 R_1. \quad (3)$$

In (3), $J_i(N_i)$ is the cylindrical Bessel function of the first (second) kind.

In order to satisfy the boundary conditions

$$E_z^{\mathrm{II}} = E_z^{inc} + E_z^{sc}, \qquad \frac{\mu_2^{-1}\partial E_z^{\mathrm{II}}}{\partial\mu} = \frac{\mu_3^{-1}\partial(E_z^{inc} + E_z^{sc})}{\partial\mu} \quad (4)$$

at the elliptical boundary $\mu = \mu_o$, we first use the translational addition theorem for the circular cylindrical wave functions [3], [7]:

$$Z_i(k_2 r_1)^{\cos}_{\sin} i\varphi_1 = \sum_{n=0}^{\infty} \frac{\varepsilon_n}{2} Z_n(k_2 r) \begin{pmatrix} J_{ni}^{c+} \cos n\varphi + J_{ni}^{s+} \sin n\varphi \\ J_{ni}^{c-} \sin n\varphi - J_{ni}^{s-} \cos n\varphi \end{pmatrix} \quad (5)$$

and then the expansion formulas connecting them with the concentric elliptical ones with respect to $xOy$ [4]:

$$Z_n(k_2 r)^{\cos}_{\sin} n\varphi = \sqrt{2\pi} \begin{pmatrix} 2/\varepsilon_n \\ 1 \end{pmatrix} \sum_{m=0}^{\infty}{}_1 j^{m-n} \frac{B_n^{e}{}_o^{o}(h, m)}{M_m^{e}{}_o^{o}(h)} \times S_{e_o m}(h, \cos\theta) Z_{e_o m}(h, \cosh\mu), \qquad (n \geq {}_1^0). \quad (6)$$

In (5) and (6), $Z_i$ and $Z_{e_o m}$ represent the Bessel function and the radial Mathieu function of the same kind, respectively, $B_n^{e(o)}(h, m)$ are the expansion coefficients for the Mathieu functions [4] ($n$, $m$ are both even or odd), $\varepsilon_0 = 1$ and $\varepsilon_n = 2$ for $n \geq 1$ is the Neumann factor, while

$$J_{ni}^{c\pm} = J_{n-i}(k_2 d)\cos(n-i)\varphi_o \pm (-1)^i J_{n+i}(k_2 d)\cos(n+i)\varphi_o \quad (7)$$

and $J_{ni}^{s\pm}$ is given by (7) if we replace cos with sin.

Substituting from (5) and (6) into (3), we express $E_z^{\mathrm{II}}$ in elliptical–cylindrical wave functions with respect to $xOy$.

By using (1) and (2) and this last expression, we satisfy (4). We then multiply both members of the resulting equations by $S_{e_o v}(h_3, \cos\theta)$ and use the orthogonal properties of the angular Mathieu functions [3], [4]. Solving the equation resulting from the second condition (4) for $P_v$ and $Q_v$, we obtain

$$\begin{matrix} P_v \\ Q_v \end{matrix} = \sqrt{2\pi}\frac{\mu_3}{\mu_2} \sum_{i=0}^{\infty}\sum_{n=0}^{\infty}{}_1\sum_{m=0}^{\infty}{}_1 j^{m-n} \times \left[ \frac{B_n^{e}{}_o^{o}(h, m) M_{mv}^{o}{}_o^{e}(h, h_3)}{M_m^{e}{}_o^{o}(h) M_v^{o}{}_o^{e}(h_3)} \frac{\dfrac{dV_{mi}^{o}{}_o^{e}(h, \cosh\mu)}{d\mu}}{\dfrac{dH_{e_o v}(h_3, \cosh\mu)}{d\mu}} \right|_{\mu=\mu_o} \times (A_i J_{ni}^{s+} \mp B_i J_{ni}^{s-}) \Bigg] - \sqrt{8\pi} j^{-v} \frac{S_{e_o v}(h_3, \cos\psi)}{M_v^{o}{}_o^{e}(h_3)} \times \left. \frac{\dfrac{dJ_{e_o v}(h_3, \cosh\mu)}{d\mu}}{\dfrac{dH_{e_o v}(h_3, \cosh\mu)}{d\mu}} \right|_{\mu=\mu_o}, \qquad (v \geq {}_1^0) \quad (8)$$

where $v$, $n$, $m$ are all three even or odd:

$$V_{mi}^{o}{}_o^{e}(h, \cosh\mu) = J_{e_o m}(h, \cosh\mu) N_i(x_3) - J_i(x_3) N_{e_o m}(h, \cosh\mu) \quad (9)$$

$$M_{mv}^{o}{}_o^{e}(h, h_3) = \int_0^{2\pi} S_{e_o m}(h, \cos\theta) S_{e_o v}(h_3, \cos\theta)\, d\theta = \pi \sum_{n=0}^{\infty}{}_1 \begin{pmatrix} 2/\varepsilon_n \\ 1 \end{pmatrix} B_n^{e}{}_o^{o}(h, m) B_n^{e}{}_o^{o}(h_3, v). \quad (10)$$

$\overset{e}{Ne}_m(\overset{e}{No}_m)$ the even (odd) radial Mathieu functions of the second kind and $\overset{o}{M}_m^{(}h) = \overset{e}{M}_{mm}^{o}(h, h)$.

Substituting next from (8) into the equation resulting from the first (4), we obtain the following two infinite linear sets for $A_i$ and $B_i$:

$$\sum_{i=0}^{\infty} \alpha_{vi}^{ec} A_i + \sum_{i=1}^{\infty} b_{vi}^{es} B_i = d_v^e, \qquad (v \geq 0)$$
$$\sum_{i=0}^{\infty} \alpha_{vi}^{os} A_i + \sum_{i=1}^{\infty} b_{vi}^{oc} B_i = d_v^o, \qquad (v \geq 1) \tag{11}$$

where

$$\begin{aligned}\alpha_{vi}^{ec(os)} \\ b_{vi}^{es(oc)}\end{aligned} = \pm(+) \sum_{n=0(1)}^{\infty} \sum_{m=0(1)}^{\infty} \times j^{m-n} \frac{B_n^{e(o)}(h, m) M_{mv}^{e(o)}(h, h_3)}{M_m^{e(o)}(h)} \times [J_{mv}^{e(o)} N_i(x_3) - J_i(x_3)\ N_{mv}^{e(o)}] \begin{bmatrix} J_{ni}^{c(s)+} \\ J_{ni}^{s(c)-} \end{bmatrix} \tag{12}$$

$$\overset{e}{d}_v^o = 2j^{-v} S_{\overset{e}{o}v}(h_3, \cos\psi) \left[ J_{\overset{e}{o}v}(h_3, \cosh\mu_o) - H_{\overset{e}{o}v}(h_3, \cosh\mu_o) \frac{\dfrac{dJ_{\overset{e}{o}v}(h_3, \cosh\mu)}{d\mu}}{\dfrac{dH_{\overset{e}{o}v}(h_3, \cosh\mu)}{d\mu}} \bigg|_{\mu=\mu_o} \right] \tag{13}$$

$$\overset{e}{Z}_{mv}^o = Z_{\overset{e}{o}m}(h, \cosh\mu_o) - \frac{\mu_3}{\mu_2} H_{\overset{e}{o}v}(h_3, \cosh\mu_o) \times \frac{\dfrac{dZ_{\overset{e}{o}m}(h, \cosh\mu)}{d\mu}}{\dfrac{dH_{\overset{e}{o}v}(h_3, \cosh\mu)}{d\mu}} \bigg|_{\mu=\mu_o}, \qquad Z = J, N \tag{14}$$

and $v$, $n$, $m$ are all even or odd.

For general values of $h(h_3 = qh,\ q = k_3/k_2)$, the sets (11) can be solved only numerically by truncation, a complicated task due to the calculation of the Mathieu functions for each different $h$. However, for small $h(\ll 1)$, a semianalytical solution is possible. After very lengthy (but straightforward) calculations, one can find expansions of the form

$$\begin{aligned}\alpha_{vi}(h) &= C_{vi} + C_{vi}^{(2)} h^2 + O(h^4) \\ b_{vi}(h) &= T_{vi} + T_{vi}^{(2)} h^2 + O(h^4) \\ d_v(h) &= D_v + D_v^{(2)} h^2 + O(h^4).\end{aligned} \tag{15}$$

The analytical expressions of the coefficients $C$, $T$, and $D$, which are different for the various superscripts [(11)–(14)], are given in the Appendix.

For the evaluation of $A_i$'s and $B_i$'s from (11), we use Cramer's rule and the expansions (15). The procedure followed is the same as in [8] and will not be repeated here. Thus, we again obtain [8, eq. (17), (18)], with the only difference that the value $q = m$ is not excluded here, while the elements $d_1, d_2, \cdots, d_n$ in the determinant $\Delta_n^{o\prime}$ are replaced by $D_1, D_2, \cdots, D_n$, respectively. Equation [8, eq. (19)] is also valid, but with superscripts and subscripts as in the present (11).

In the special case with $d = 0$, or $d = 0$ and $h \ll 1$ or $\varphi_o = 0, \pi$, we obtain various simplified expressions similar to those described in detail in [7] for the corresponding interior problem. Thus, for $d = 0$, or $d = 0$ and $h \ll 1$, the various quantities appearing here become identical with the corresponding ones in [6] (for $\mu_2 = \mu_3$ and $h_3 \simeq h$).

For $h = 0$, our results agree with those independently obtained for the eccentric circular geometry. Finally, for $h = 0$ and $d = 0$, they become well known for two coaxial circular cylinders.

The former observations consist of a check on the accuracy of our results.

*2) The Scattered Far-Field:* By using formula [3], [4]

$$S_{\overset{e}{o}m}(h_3, \cos\theta) Z_{\overset{e}{o}m}(h_3, \cosh\mu) = \sqrt{\frac{\pi}{2}} \sum_{\ell=0}^{\infty} j^{\ell-m} \overset{e}{B}_{\ell}^{o}(h_3, m)_{\sin}^{\cos} \ell\varphi Z_\ell(k_3 r) \tag{16}$$

in (2) and the asymptotic expansion for the Hankel functions, we obtain the scattered far-field expression and then the differential $[\sigma(\varphi)]$, backscattering or radar $(\sigma_b)$, forward $(\sigma_f)$ and total scattering $(Q_t)$ cross sections [6], as shown in (17)–(19) at the bottom of the page, and $m$, $\ell$ are both even or odd.

The coefficients $P_m$ and $Q_m$ are given in (8). By substituting the expansions for the various quantities for small $h$, we obtain after lengthy and laborious calculations, relations of the form

$$\begin{aligned}P_m(h) &= P_m^o + P_m^{(2)} h^2 + O(h^4) \\ Q_m(h) &= Q_m^o + Q_m^{(2)} h^2 + O(h^4)\end{aligned} \tag{20}$$

$$\sigma(\varphi) = \frac{|G(\varphi)|^2}{k_3}$$
$$\sigma_b = \frac{2\pi |G(\psi + \pi)|^2}{k_3}$$
$$\sigma_f = \frac{2\pi |G(\psi)|^2}{k_3} \tag{17}$$
$$Q_t = \frac{\pi(2|P_o|^2 [B_0^e(h_3, 0)]^2 + \sum_{m=1}^{\infty} \{|P_m|^2 [B_m^e(h_3, m)]^2 + |Q_m|^2 [B_m^o(h_3, m)]^2\})}{k_3} \tag{18}$$
$$G(\varphi) = \sum_{m=0}^{\infty} \sum_{\ell=0}^{\infty} j^{2\ell-m} [P_m B_\ell^e(h_3, m) \cos\ell\varphi + Q_m B_\ell^o(h_3, m) \sin\ell\varphi] \tag{19}$$

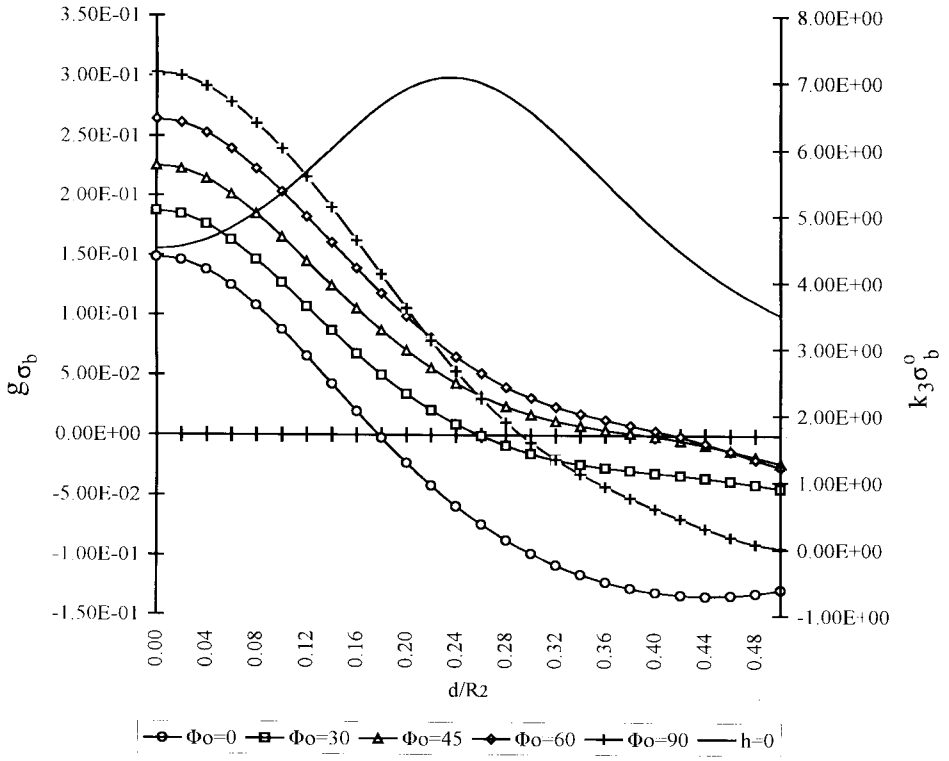


Fig. 2. Backscattering cross section for $R_1/R_2 = 0.5$, $R_2/\lambda_3 = 0.5$, $\psi - \varphi_o = 90°$, $\varepsilon_2/\varepsilon_3 = 2.54$ (metallic inner cylinder, $E$ wave).

with the expansion coefficients given in the Appendix. Analogous expansions are obtained for $G(\varphi)$, $\sigma(\varphi)$, and $Q_t$, as shown in (21)–(24) at the bottom of the page, where Re is the real part and (—) the conjugate quantity. We write $\sigma(\varphi)$, $Q_t$ as

$$\begin{aligned}\sigma(\varphi) &= \sigma^o(\varphi)[1 + g_\sigma(\varphi)h^2 + O(h^4)] \\ Q_t &= Q_t^o[1 + g_{Q_t}h^2 + O(h^4)]\end{aligned} \tag{25}$$

where

$$g_\sigma(\varphi) = \frac{\sigma^{(2)}(\varphi)}{\sigma^o(\varphi)} \quad g_{Q_t} = \frac{Q_t^{(2)}}{Q_t^o}. \tag{26}$$

Our results were verified by the forward scattering theorem [6].

### B. H-Wave Polarization

The incident wave $H_z^{\text{inc}}$ and the scattered field $H_z^{sc}$ are again given by (1), (2), respectively. The field $H_z^{\text{II}}$, satisfying the boundary condi-

$$G^o(\varphi) = P_0^o + \sum_{m=1}^{\infty} j^m \left( P_m^o \cos m\varphi + \frac{Q_m^o \sin m\varphi}{m} \right) \tag{21}$$

$$\begin{aligned}G^{(2)}(\varphi) = &\sum_{m=0}^{\infty} j^m \left\{ q^2 P_m^o \left[ \frac{\delta_m}{16(m-1)} \cos(m-2)\varphi - \frac{\cos m\varphi}{\tau_m} - \frac{1}{8\varepsilon_m(m+1)} \cos(m+2)\varphi \right] + P_m^{(2)} \cos m\varphi \right\} \\ &+ \sum_{m=1}^{\infty} \frac{j^m}{m} \left\{ q^2 Q_m^o \left[ \frac{\delta_{m-1}}{16(m-1)} \sin(m-2)\varphi + \frac{\sin m\varphi}{\tau_m'} - \frac{1}{16(m+1)} \sin(m+2)\varphi \right] + Q_m^{(2)} \sin m\varphi \right\}, \\ &q = \frac{k_3}{k_2},\ \tau_m = 8(m^2-1),\ m \neq 1,\ \tau_1 = -32,\ \tau_m' = \tau_m,\ m \geq 2,\ \tau_1' = \frac{32}{3}\end{aligned} \tag{22}$$

$$\begin{aligned}\sigma^o(\varphi) &= \frac{|G^o(\varphi)|^2}{k_3}, \\ \sigma^{(2)}(\varphi) &= \frac{2\text{Re}[G^o(\varphi)\overline{G^{(2)}}(\varphi)]}{k_3} \\ Q_t^o &= \frac{\pi \left[ 2|P_0^o|^2 + \sum_{m=1}^{\infty} \left\{ |P_m^o|^2 + \frac{|Q_m^o|^2}{m^2} \right\} \right]}{k_3} \\ Q_t^{(2)} &= \frac{2\pi \left[ 2\,\text{Re}(P_0^o \overline{P_0^{(2)}}) + q^2 \frac{|P_0^o|^2}{4} + \sum_{m=1}^{\infty} \left\{ \text{Re}\left[ P_m^o \overline{P_m^{(2)}} + \frac{Q_m^o \overline{Q_m^{(2)}}}{m^2} \right] - q^2 \left[ \frac{|P_m^o|^2}{\tau_m} - \frac{|Q_m^o|^2}{m^2 \tau_m'} \right] \right\} \right]}{k_3}\end{aligned} \tag{23, 24}$$

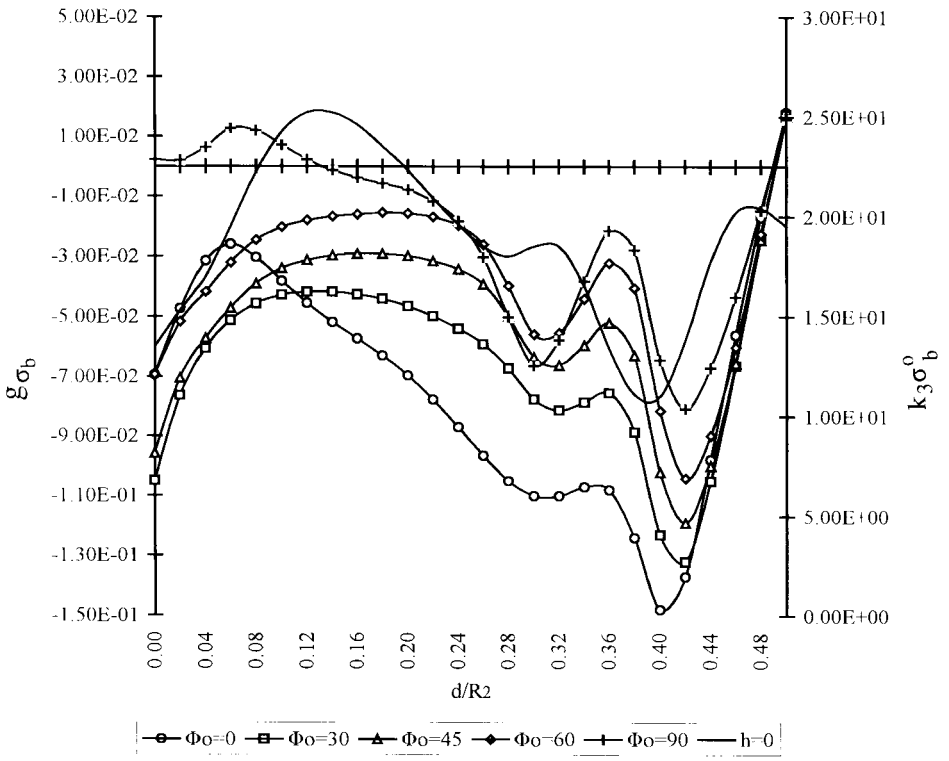


Fig. 3. Backscattering cross section for $R_1/R_2 = 0.5$, $R_2/\lambda_3 = 0.7$, $\psi - \varphi_o = 60°$, $\varepsilon_2/\varepsilon_3 = 5.5$ (metallic inner cylinder, $H$ wave).

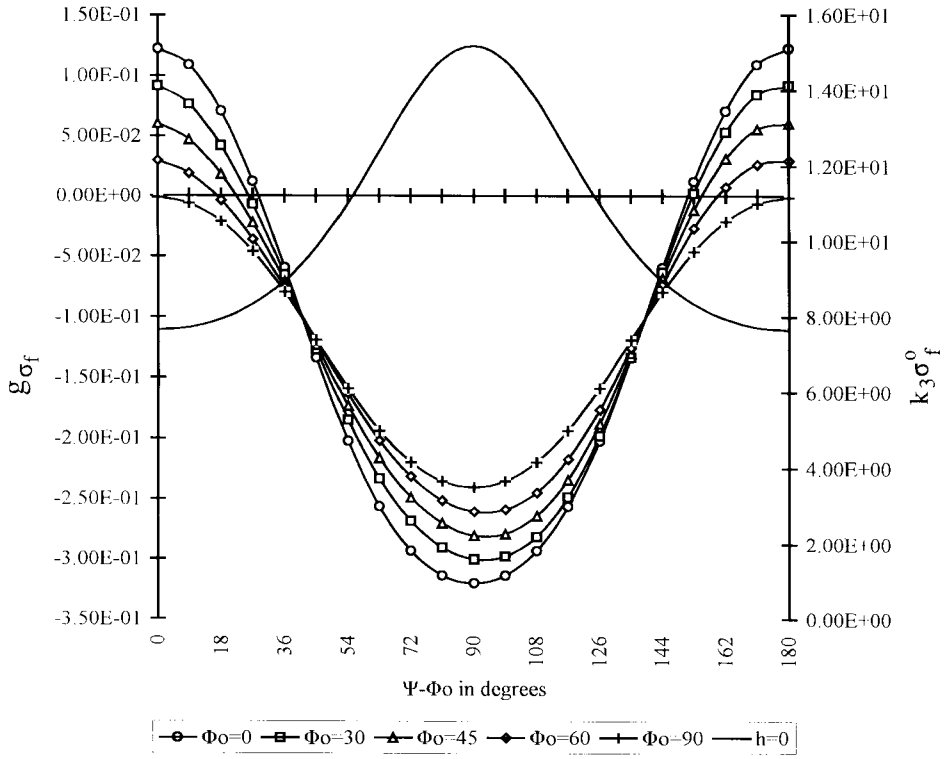


Fig. 4. Forward scattering cross section for $R_1/R_2 = 0.5$, $R_2/\lambda_3 = 0.3$, $d/R_2 = 0.4$, $\varepsilon_2/\varepsilon_3 = 2.54$ (metallic inner cylinder, $E$ wave).

tion $\partial H_z^{\mathrm{II}}/\partial r_1 = 0$ at $r_1 = R_1$, is given by (3) with $N_i(x_3)$, $J_i(x_3)$ replaced by $N_i'(x_3)$, $J_i'(x_3)$, respectively (derivatives with respect to the argument). In (4) and the following relations, we replace $E$, $\mu_2$, $\mu_3$ with $H$, $\varepsilon_2$, $\varepsilon_3$, respectively. Thus we again obtain (5)–(26), with the aforementioned changes.

## III. Dielectric Inner Cylinder

If the inner cylinder is dielectric with parameters $\varepsilon_1$, $\mu_1$, and $k_1$, there is also a field inside it, which in the $E$-wave case is expressed as

$$E_z^{\mathrm{I}} = \sum_{i=0}^{\infty} J_i(k_1 r_1)(U_i \cos i\varphi_1 + W_i \sin i\varphi_1). \qquad (27)$$

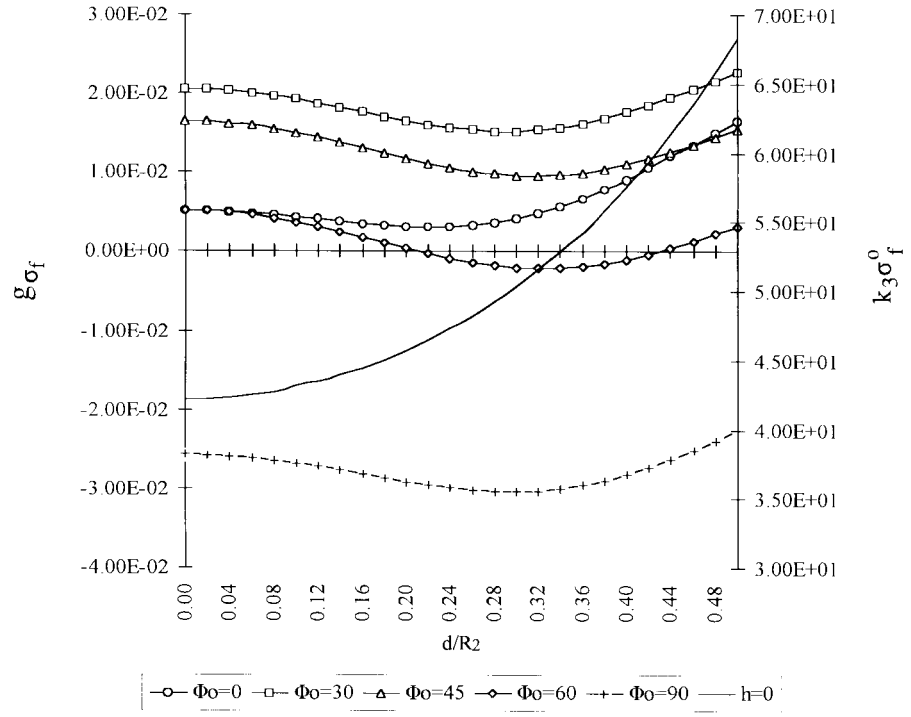


Fig. 5. Forward scattering cross section for $R_1/R_2 = 0.5$, $R_2/\lambda_3 = 0.5$, $\psi - \varphi_o = 60°$, $\varepsilon_1/\varepsilon_3 = 5.5$, $\varepsilon_2/\varepsilon_3 = 2.54$ (dielectric inner cylinder, $H$ wave).

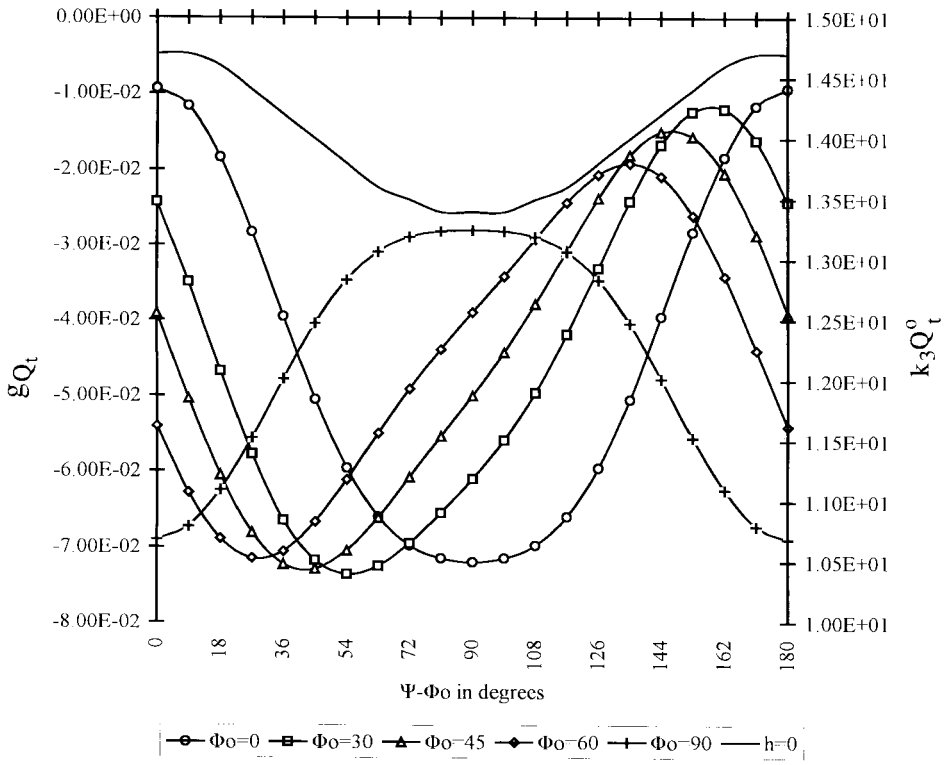


Fig. 6. Total scattering cross section for $R_1/R_2 = 0.5$, $R_2/\lambda_3 = 0.3$, $d/R_2 = 0.4$, $\varepsilon_1/\varepsilon_3 = 5.5$, $\varepsilon_2/\varepsilon_3 = 2.54$ (dielectric inner cylinder, $E$ wave).

The field $E_z^{\mathrm{II}}$, which satisfies the boundary conditions

$$E_z^{\mathrm{I}} = E_z^{\mathrm{II}}, \frac{\mu_1^{-1}\partial E_z^{\mathrm{I}}}{\partial r_1} = \frac{\mu_2^{-1}\partial E_z^{\mathrm{II}}}{\partial r_1} \tag{28}$$

at $r_1 = R_1$, has the expression

$$E_z^{\mathrm{II}} = \sum_{i=0}^{\infty} [J_i(k_2 r_1) p_i^E(x_1, x_3) - q_i^E(x_1, x_3) N_i(k_2 r_1)] \times (A_i \cos i\varphi_1 + B_i \sin i\varphi_1) \tag{29}$$

where

$$\begin{matrix} U_i \\ W_i \end{matrix} = \frac{J_i(x_3) p_i^E(x_1, x_3) - q_i^E(x_1, x_3) N_i(x_3)}{J_i(x_1)} \begin{bmatrix} A_i \\ B_i \end{bmatrix}, \quad x_1 = k_1 R_1, \; x_2 = k_2 R_1 \tag{30}$$

$$\begin{matrix} p_i^E(x_1, x_3) \\ q_i^E(x_1, x_3) \end{matrix} = J_i'(x_1) \begin{bmatrix} N_i(x_3) \\ J_i(x_3) \end{bmatrix} - \frac{k_2\mu_1}{k_1\mu_2} J_i(x_1) \begin{bmatrix} N_i'(x_3) \\ J_i'(x_3) \end{bmatrix}. \tag{31}$$

The incident and scattered fields are again given by (1) and (2), respectively. The remaining equations are the same as for a metallic inner cylinder, with the only difference being that $N_i(x_3)$ and $J_i(x_3)$ are now replaced everywhere by $p_i^E$ and $q_i^E$, respectively, as can be seen from (3) and (29).

For the $H$-wave case (27)–(31) are valid again, with $E$, $\mu_1$, $\mu_2$ replaced by $H$, $\varepsilon_1$, $\varepsilon_2$, respectively. The remainder of the steps are identical with those for the $E$-wave case, but with the difference that $\mu_2$ and $\mu_3$ should be replaced by $\varepsilon_2$, $\varepsilon_3$, respectively, in (4) and the relations following it.

## IV. Numerical Results and Discussion

In Figs. 2–6 the $g$'s for the various scattering cross sections of the configuration of Fig. 1 are plotted for various values of the parameters and for both polarizations. In each figure, we also plot the corresponding scattering cross section for $h = 0$ (eccentric circular geometry), which depends only on the difference between the angles $\psi$ and $\varphi_o$ and not on their distinct values, such as $h \neq 0$. In this latter case, each curve is plotted for one distinct value of $\varphi_o$, which when added to the known $\psi - \varphi_o$ gives the corresponding $\psi$. Thus it is very easy to calculate the scattering cross sections by the formula $S(h) = S(0)[1 + gh^2 + O(h^4)]$, for each small $h$ and for the values of the parameters used. $S(0)$ corresponds to the eccentric circular geometry.

In a more analytical sense, in Figs. 2 and 3 we plot $k_3\sigma_b^o$ (for $h = 0$) as well as the coefficients $g_{\sigma_b}$. The same is done in Figs. 4 and 5 for $k_3\sigma_f^o$ and $g_{\sigma_f}$, and finally in Fig. 6 for $k_3 Q_t^o$ and $g_{Q_t}$. In each figure, we have used equal permeabilities in all regions, while $\lambda_3 = 2\pi/k_3$ is the wavelength in Region III.

A result expected from reciprocity, is that $\sigma_f$ has the same values, i.e., equal $g$'s for incidence angles differing by $\pi$ (also with a sum equal to $\pi$, for $\varphi_o = 0,\ \pi/2,\ \pi,\ 3\pi/2$, or for $h = 0$). This also holds for $Q_t$ and is the reason for which $\psi - \varphi_o$ in Figs. 4 and 6 varies only from $0 - \pi$.

Our present approximate results are verified with very good accuracy by the independent, purely numerical, solution of the same problem for various small values of $h$ by truncation of (11). The percentage of error between the two methods is less than 1%, even for $h$ up to 0.8, at least for the values of the parameters used in Figs. 2–6, so the restriction $h \ll 1$ is not so severe as may have first appeared. The terms omitted are of the order $h^4$, so $h$ can take relatively large values in our solution.

---

$$\begin{aligned} C_{vi}^{ec} &= \pm u_{vvi} J_{vi}^{c+s-} \\ T_{vi}^{es} &= \pm u_{vvi} J_{vi}^{c+s-} \\ C_{vi}^{os} &= \frac{\tanh \mu_o}{v}\, u_{vvi} J_{vi}^{s+c-} \\ T_{vi}^{oc} &= \frac{\tanh \mu_o}{v}\, u_{vvi} J_{vi}^{s+c-} \end{aligned} \tag{A1}$$

$$\begin{aligned} \begin{bmatrix} C_{vi}^{(2)ec} \\ T_{vi}^{(2)es} \end{bmatrix} &= (\pm) \left(\frac{\tanh \mu_o}{v}\right) \left\{ \begin{bmatrix} -\dfrac{\delta_v}{16(v-1)} \\ -\dfrac{\delta_{v-1}}{16(v-1)} \end{bmatrix} [(1-q^2)u_{v-2,v,i} + u_{vvi}] \begin{bmatrix} J_{v-2,i}^{c+s-} \\ J_{v-2,i}^{s+c-} \end{bmatrix} + \begin{bmatrix} \dfrac{1}{8\varepsilon_v(v+1)} \\ \dfrac{1}{16(v+1)} \end{bmatrix} \times [(1-q^2)u_{v+2,v,i} + u_{vvi}] \right. \\ &\quad \cdot \begin{bmatrix} J_{v+2,i}^{c+s-} \\ J_{v+2,i}^{s+c-} \end{bmatrix} + \left[ \begin{pmatrix} -\dfrac{\delta_v}{16(v-1)} \\ -\dfrac{\delta_{v-1}(v-2)}{16v(v-1)} \end{pmatrix} \left(u_{v-2,v,i} - q\,\frac{\mu_3}{\mu_2}\, s_{v-2,v,i}\right) + \begin{pmatrix} -\dfrac{1}{\tau_v} \\ \dfrac{1}{\tau_v'} \end{pmatrix} (1+q^2)u_{vvi} \right. \\ &\quad + \begin{bmatrix} \dfrac{1}{8\varepsilon_v(v+1)} \\ \dfrac{v+2}{16v(v+1)} \end{bmatrix} \left(u_{v+2,v,i} - q\,\frac{\mu_3}{\mu_2}\, s_{v+2,v,i}\right) \\ &\quad \left. \left. + \begin{pmatrix} 0 \\ \left\{ \dfrac{q}{x_4^3}\,\dfrac{\mu_3}{\mu_2} \left[\dfrac{H_v(x_4)}{H_v'(x_4)}\right]^2 w_{vi}' - \dfrac{1}{qx_2^3}\,\dfrac{\mu_3}{\mu_2}\,\dfrac{H_v(x_4)}{H_v'(x_4)}\, w_{vi} \right\} \end{pmatrix} \right] \begin{pmatrix} J_{vi}^{c+s-} \\ J_{vi}^{s+c-} \end{pmatrix} \right\} \end{aligned} \tag{A2}$$

$$D_v^e = 2j^{-v} Y_{vv} \begin{pmatrix} \cos v\psi \\ \tanh \mu_o \sin v\psi / v \end{pmatrix} \tag{A3}$$

$$\begin{aligned} \begin{matrix} D_v^{(2)e} \\ D_v^{(2)o} \end{matrix} &= 2j^{-v} q^2 \left(\frac{1}{\dfrac{\tanh \mu_o}{v}}\right) \left\{ \left[ \begin{bmatrix} \dfrac{\delta_v}{16(v-1)} \\ \dfrac{\delta_{v-1}}{16(v-1)} \end{bmatrix} \begin{matrix} \cos \\ \sin \end{matrix} (v-2)\psi - \begin{bmatrix} \dfrac{1}{8\varepsilon_v(v+1)} \\ \dfrac{1}{16(v+1)} \end{bmatrix} \begin{matrix} \cos \\ \sin \end{matrix} (v+2)\psi \right] Y_{vv} \right. \\ &\quad + \begin{bmatrix} -\dfrac{\delta_v}{16(v-1)} \\ -\dfrac{\delta_{v-1}(v-2)}{16v(v-1)} \end{bmatrix} (Y_{v-2,v} - \Phi_{v-2,v,v}) + \begin{pmatrix} -\dfrac{2}{\tau_v} \\ \dfrac{2}{\tau_v'} \end{pmatrix} Y_{vv} \\ &\quad \left. + \begin{bmatrix} \dfrac{1}{8\varepsilon_v(v+1)} \\ \dfrac{v+2}{16v(v+1)} \end{bmatrix} (Y_{v+2,v} - \Phi_{v+2,v,v}) - \begin{bmatrix} 0 \\ \dfrac{Y_{vv}}{x_4^3}\,\dfrac{H_v(x_4)}{H_v'(x_4)} \end{bmatrix} \right\} \begin{matrix} \cos \\ \sin \end{matrix} v\psi \end{aligned} \tag{A4}$$

$$\begin{matrix} P_v^o \\ Q_v^o \end{matrix} = \sum_{i=0}^{\infty} \left[ K_{vi}^{os\,ec} A_i^o + \Lambda_{vi}^{oc\,es} B_i^o \right] - j^{-v(\varepsilon_v)} \sqrt{\frac{2}{\pi}} \frac{J_v'(x_4)}{H_v'(x_4)} \begin{matrix} \cos \\ \sin \end{matrix} v\psi \tag{A9}$$

$$\begin{aligned} \begin{matrix} P_v^{(2)} \\ Q_v^{(2)} \end{matrix} &= \sum_{i=0}^{\infty} \left[ K_{vi}^{os\,ec} A_i^{(2)} + K_{vi}^{(2)os\,ec} A_i^o + \Lambda_{vi}^{oc\,es} B_i^{(2)} + \Lambda_{vi}^{(2)oc\,es} B_i^o \right] - \begin{matrix} (\varepsilon_v) \\ (2v) \end{matrix} j^{-v} \sqrt{\frac{2}{\pi}}\, q^2 \\ &\times \left\{ \frac{J_v'(x_4)}{H_v'(x_4)} \left[ \begin{matrix} \left[ \dfrac{\delta_v}{16(v-1)} \right] \\ \left[ \dfrac{\delta_{v-1}}{16v(v-1)} \right] \end{matrix} \begin{matrix} \cos \\ \sin \end{matrix} (v-2)\psi - \begin{matrix} \left[ \dfrac{1}{8\varepsilon_v(v+1)} \right] \\ \left[ \dfrac{1}{16(v+1)} \right] \end{matrix} \begin{matrix} \cos \\ \sin \end{matrix} (v+2)\psi \right] \right. \\ &+ \left[ \begin{matrix} \left[ \dfrac{\delta_v}{16(v-1)} \right] \\ -\left[ \dfrac{\delta_{v-1}(v-2)}{16v(v-1)} \right] \end{matrix} Y_{v-2,\,v}' + \begin{matrix} (0) \\ \left[ \dfrac{Y_{vv}}{x_4^3 H_v'(x_4)} \right] \end{matrix} + \begin{matrix} \left( \dfrac{1}{\tau_v} \right) \\ \left( -\dfrac{1}{\tau_v'} \right) \end{matrix} \frac{J_v'(x_4)}{H_v'(x_4)} \right. \\ &\left. \left. + \begin{matrix} \left[ \dfrac{1}{8\varepsilon_v(v+1)} \right] \\ \left[ \dfrac{v+2}{16v(v+1)} \right] \end{matrix} Y_{v+2,\,v}' \right] \begin{matrix} \cos \\ \sin \end{matrix} v\psi \right\} \end{aligned} \tag{A10}$$

where

$$\begin{matrix} K_{vi}^{ec} \\ \Lambda_{vi}^{es} \end{matrix} = \pm \frac{\varepsilon_v}{2H_v'(x_4)} \sqrt{\frac{2}{\pi}} \frac{\mu_3}{q\mu_2} w_{vi}' J_{vi}^{s-\,c+}$$

$$\begin{matrix} K_{vi}^{os} \\ \Lambda_{vi}^{oc} \end{matrix} = \frac{v}{H_v'(x_4)} \sqrt{\frac{2}{\pi}} \frac{\mu_3}{q\mu_2} w_{vi}' J_{vi}^{c-\,s+} \tag{A11}$$

$$\begin{aligned} \begin{bmatrix} K_{vi}^{(2)ec} \\ \Lambda_{vi}^{(2)es} \end{bmatrix} &= \begin{bmatrix} \left[ \pm \dfrac{1}{H_v'(x_4)} \right] \\ \left[ \dfrac{v}{H_v'(x_4)} \right] \end{bmatrix} \sqrt{\frac{2}{\pi}} \frac{\mu_3}{q\mu_2} \left\{ \begin{bmatrix} \left[ -\dfrac{\delta_v}{16(v-1)} \right] \\ \left[ -\dfrac{\delta_{v-1}}{16(v-1)} \right] \end{bmatrix} [(1-q^2) w_{v-2,\,i}' + w_{vi}'] \begin{pmatrix} J_{v-2,\,i}^{s-\,c+} \\ J_{v-2,\,i}^{c-\,s+} \end{pmatrix} + \frac{1}{16(v+1)} \times [(1-q^2) w_{v+2,\,i}' + w_{vi}'] \right. \\ &\cdot \begin{pmatrix} J_{v+2,\,i}^{s-\,c+} \\ J_{v+2,\,i}^{c-\,s+} \end{pmatrix} + \begin{bmatrix} \left[ -\dfrac{\delta_v}{16(v-1)} \right] \\ \left[ -\dfrac{\delta_{v-1}(v-2)}{16v(v-1)} \right] \end{bmatrix} \left[ w_{v-2,i}' - q^2 \frac{H_{v-2}'(x_4)}{H_v'(x_4)} w_{vi}' \right] + \begin{pmatrix} \left( -\dfrac{\varepsilon_v}{2\tau_v} \right) \\ \left( \dfrac{1}{\tau_v'} \right) \end{pmatrix} \times (1-2q^2) w_{vi}' \\ &\left. + \begin{bmatrix} \left[ \dfrac{1}{16(v+1)} \right] \\ \left[ \dfrac{v+2}{16v(v+1)} \right] \end{bmatrix} \left[ w_{v+2,\,i}' - q^2 \frac{H_{v+2}'(x_4)}{H_v'(x_4)} w_{vi}' \right] \left\{ \frac{1}{x_2^3} \left[ w_{vi} - \frac{H_v(x_4)}{qH_v'(x_4)} w_{vi}' \right] \right\} \right] \begin{pmatrix} J_{vi}^{s-\,c+} \\ J_{vi}^{c-\,s+} \end{pmatrix} \end{aligned} \tag{A12}$$

$$Y_{mv}' = \frac{J_m'(x_4) H_v'(x_4) - H_m'(x_4) J_v'(x_4)}{[H_v'(x_4)]^2} \tag{A13}$$

## APPENDIX

The analytical expressions for the expansion coefficients $C$, $T$, $D$, and $P$, $Q$, appearing in (15) and (20), respectively, are obtained after very lengthy but straightforward calculations, by using the definitions and relations for Mathieu functions [4], [6]. Thus we obtain for a metallic inner cylinder and for the $E$-wave polarization as shown in (A1)–(A4) at the bottom of the previous page, where

$$u_{mvi} = w_{mi} - \frac{\mu_3}{q\mu_2} \frac{H_v(x_4)}{H_v'(x_4)} w_{mi}'$$

$$s_{mvi} = X_{mv} w_{vi}' \tag{A5}$$

$$w_{mi} = J_m(x_2) N_i(x_3) - J_i(x_3) N_m(x_2)$$

$$w_{mi}' = J_m'(x_2) N_i(x_3) - J_i(x_3) N_m'(x_2) \tag{A6}$$

$$Y_{mv} = J_m(x_4) - \frac{H_v(x_4)}{H_v'(x_4)} J_m'(x_4) \tag{A7}$$

$$X_{mv} = \frac{H_m(x_4) H_v'(x_4) - H_v(x_4) H_m'(x_4)}{[H_v'(x_4)]^2}$$

$$\Phi_{mvv} = X_{mv} J_v'(x_4) \tag{A8}$$

and $\delta_0 = \delta_1 = 0$, $\delta_v = 1$ for $v \geq 2$, while $\tau_v = 8(v^2 - 1)$, $(v \neq 1)$, $\tau_1 = -32$, $\tau_v' = \tau_v$, $(v \geq 2)$, $\tau_1' = 32/3$. Also, $q = k_3/k_2$, $x_2 = k_2 R_2$, $x_3 = k_2 R_1$, $x_4 = k_3 R_2$, and $H_v$ is the cylindrical Hankel function of the second kind.

The expansion coefficients for $P$ and $Q$ (20) are shown in (A9)–(A13) at the top of the page, while $A_i^o$, $B_i^o$ and $A_i^{(2)}$, $B_i^{(2)}$ are obtained from the solution of (11).

The same relations are also valid for a metallic inner cylinder and the $H$-wave polarization, as well as for a dielectric inner cylinder and both polarizations, with the changes which are referred to in the relative sections.

## REFERENCES


[1] A. Sebak, H. A. Ragheb, and L. Shafai, "Plane wave scattering by dielectric elliptic cylinder coated with nonconfocal dielectric," *Radio Sci.,* vol. 29, pp. 1393–1401, Nov./Dec. 1994.

[2] A. R. Sebak, "Electromagnetic scattering by two parallel dielectric elliptic cylinders," *IEEE Trans. Antennas Propagat.,* vol. 42, pp. 1521–1527, Nov. 1994.

[3] J. A. Stratton, *Electromagnetic Theory.* New York: McGraw-Hill, 1941.

[4] P. M. Morse and H. Feshbach, *Methods of Theoretical Physics.* New York: McGraw-Hill, 1953.

[5] H. A. Ragheb, L. Shafai, and M. Hamid, "Plane wave scattering by a conducting elliptic cylinder coated by a nonconfocal dielectric," *IEEE Trans. Antennas Propagat.,* vol. 39, pp. 218–223, Feb. 1991.

[6] J. A. Roumeliotis, H. K. Manthopoulos, and V. K. Manthopoulos, "Electromagnetic scattering from an infinite circular metallic cylinder coated by an elliptic dielectric one," *IEEE Trans. Microwave Theory Tech.,* vol. 41, pp. 862–869, May 1993.

[7] J. A. Roumeliotis and S. P. Savaidis, "Cutoff frequencies of eccentric circular-elliptic metallic waveguides," *IEEE Trans. Microwave Theory Tech.,* vol. 42, pp. 2128–2138, Nov. 1994.

[8] ——, "Scattering by an infinite circular dielectric cylinder coating eccentrically an elliptic metallic one," *IEEE Trans. Antennas Propagat.,* vol. 44, pp. 757–763, May 1996.


# Enhancements of the Spectral-Domain Approach for Analysis of Microstrip Y-Junction

B. L. Ooi, M. S. Leong, P. S. Kooi, and T. S. Yeo

***Abstract*— Some enhancements of the spectral-domain approach in the polar coordinate are described. A simple and efficient algorithm is devised to numerically evaluate the contribution of the oscillatory tail of the two-dimensional (2-D) Sommerfeld integral. For the first time, four new vectorized basis functions are proposed. Good agreement is obtained between the simulated results and the measured data for a microstrip Y-junction in the 4–12 GHz range.**

***Index Terms*—Microstrip, numerical integration, planar transmission lines, spectral-domain method.**

## I. INTRODUCTION

The numerical computation of the Sommerfeld integrals in the polar coordinate has been dealt with by many authors [1], [2]. In 1992, Dvorak *et al.* [1], [2] have developed some methods to compute the two-dimensional (2-D) Sommerfeld integrals in the polar coordinate. Their methods have certain drawbacks in that: 1) there is a large amount of analytical manipulation that ought to be done before the tails of the 2-D Sommerfeld integrals can be evaluated and 2) the evaluation of the tails of the 2-D Sommerfeld integrals often involves tedious and complicated functions which are not applicable for any arbitrary basis functions. Although the fast Fourier transform (FFT) algorithm [3] can be used to improve the convergence of the Sommerfeld integrals for the modeling of nonrectangular discontinuity, the FFT algorithm fails to achieve good solution because the discretization scheme cannot assure that all points are located in the cross-points of a regular grid. Moreover, the modeling of a nonrectangular discontinuity with rectangular cells is ineffective because the use of a large number of elements is necessary.

Of course, the Rao's vector basis function [4] can always be used to eliminate the staircase approximation. However, this basis function is not very competitive as compared to the rectangular basis function and should be used only if it is absolutely necessary. In 1993, Eibert [6] provided an enhancement on Rautio's basis function [5] by using a new expansion function consisting of one triangle and two adjacent rectangles with arbitrary orientation within the plane of the circuit. In his method, a removable singularity, which requires extra analytical manipulations, appears in the Fourier transform of a linear distribution with triangular support [7] when the polar transform vector $\lambda = \sqrt{k_x^2 + k_y^2}$ is perpendicular or parallel to any edge of the triangle [8].

The purpose of this paper is to introduce some enhancements of the spectral-domain approach and to use four new vectorized expansion functions based on an extension on Eibert's work, for the analysis of an arbitrarily angled microstrip Y-junction. This paper further describes a new general algorithm for evaluating the 2-D polar spectral integrals which arise. Finally, some numerical results will be presented and discussed.

## II. GENERAL FORMULATIONS

An arbitrarily angled microstrip Y-junction consisting of a thickness $h$ and a lossless nonmagnetic relative dielectric permittivity $\varepsilon_r$ is shown in Fig. 1. The global coordinate system with the $u$-direction being along the arm and the $v$-direction being orthogonal to the $u$-direction, is also presented in Fig. 1.

In our analysis, four types of current expansion functions are utilized in the method. They are the arbitrarily oriented pseudo-exponential window traveling wave (PEW) functions, the vectorized roof-top subdomain functions (T), the arbitrarily oriented rectangular subdomain functions (R) and the vectorized triangular–rectangular subdomain functions (RT).

### *A. Arbitrarily Oriented Pseudo-Exponential Window Traveling Wave (PEW)*

This current expansion function is an extension of Cicchetti's work [9] to the case of arbitrary orientation. The Fourier transforms of the basis functions can be obtained by application of linear coordinate transformations and shifting property of Fourier transform to the direct solutions of the Fourier integrals [9] for the corresponding functions which are rotated and shifted to an appropriate location within the $xy$-plane. The PEW, which is used to simulate the incoming and outgoing currents on the feedlines, allows us to extract the scattering parameters without any de-embedding since the scattering parameters are embedded in the coefficients of the traveling wave functions.

Manuscript received March 8, 1996; revised June 20, 1997.

The authors are with the Department of Electrical Engineering, National University of Singapore, Singapore.

Publisher Item Identifier S 0018-9480(97)07115-9.